NASA CR-132525



AIRESEARCH MANUFACTURING COMPANY
OF CALIFORNIA
A Division of The Garrett Corporation
2525 W. 190th Street, Torrance, Calif. 90509

# HYPERSONIC RESEARCH ENGINE PROJECT - PHASE II SOME COMBUSTOR TEST RESULTS OF NASA AEROTHERMODYNAMIC INTEGRATION MODEL (U)

DATA ITEM NO. 54.14
NASA CONTRACT NO. NAS1-6666

74-10818



ISSUED MAY 1975



Number of pages 26

Prepared by Y. H. Sun et al

Original date 26 September 1974

Edited by Staff

Approved by Q. G. Duff
for Edward N. Harris
HRE Program Manager

Prepared for

National Aeronautics and Space Administration
Langley Research Center
Hampton, Virginia 23365



(NASA-CR-132525) HYPERSONIC RESEARCH ENGINE PROJECT. PHASE 2: SOME COMBUSTOR TEST RESULTS OF NASA AEROTHERMODYNAMIC INTEGRATION MODEL (AiResearch Mfg. Co., Torrance, Calif.) 26 p HC $3.75 CSCL 21E G3/07

N75-24738

Unclas
24180

## FOREWORD

This analytical report is submitted to the NASA Langley Research Center in compliance with Paragraph 5.7.3.2.1 of NASA Statement of Work L-4947-B (Revised).

The contents of this report were previously presented as a scientific paper before the 11th JANNAF (Joint Army, Navy, NASA, and Air Force) Combustion Conference held at the Jet Propulsion Laboratory in Pasadena, California, on September 12, 1974.

CONTENTS

## ILLUSTRATIONS

[redacted]

# SOME COMBUSTOR TEST RESULTS OF NASA AEROTHERMODYNAMIC INTEGRATION MODEL (AIM/HRE) (U)

YUNG H. SUN, ALBERT E. GAEDE and WALTER C. SAINIO

AiResearch Manufacturing Company of California
Torrance, California

## ABSTRACT

(U) The Aerothermodynamic Integration Model (AIM) was built under the Hypersonic Research Engine Contract NASI-6666, NASA Langley Research Center. A program was initiated in February 1967 to develop a research ram jet engine for operation between Mach 3 and 8. The objectives were to conduct ground-based and flight experiments which would provide the data required to advance the technology of hypersonic air-breathing propulsion systems as well as to evaluate facility and testing techniques. The engine was tested at the NASA Hypersonic Tunnel Facility (HTF) at the Plum Brook Station of the Lewis Research Center with synthetic air at Mach 5, 6, and 7. The hydrogen fuel was heated to 1500°R prior to injection to simulate a regeneratively cooled system.

(C) Combustor efficiencies up to 95 percent at Mach 6 were achieved. Combustor process in terms of effectiveness, pressure integral factor, total pressure recovery and Crocco's pressure-area relationship are presented and discussed. One dimensional analyses of test results confirmed that no significant difference in performance existed at Mach 6 between supersonic and subsonic combustion. Interactions between inlet-combustor, combustor stages, combustor-nozzle, and the effects of altitude, combustor step, and struts were observed and analyzed.

## INTRODUCTION

(U) This paper presents some combustor test results of the NASA Aerothermodynamic Integration Model (AIM) which was designed, developed and built by AiResearch Manufacturing Company of California, under the Hypersonic Research Engine Contract with the NASA Langley Research Center. Work was initiated on the contract in February 1967. The basic objectives were to conduct ground-based and flight experiments which would provide realistic and useful information needed to advance the technology of hypersonic propulsion systems, and to evaluate requirements for future ground test facilities and experimental techniques. The AIM is a research oriented ramjet designed for operation at flight Mach numbers from 3 to 8. The engine size was selected primarily from the constraints imposed by the X-15 airplane which was originally scheduled as the flight test vehicle. The AIM was designed to operate with supersonic combustion at free-stream Mach Numbers from 6 to 8, and with subsonic combustion from Mach 3 to 6 to achieve best engine performance.







[redacted]

[redacted]

(U) A total of 6-1/2 months of engine testing has been completed with 110 minutes of running time accumulated. Among numerous investigations conducted, the following topics pertinent to combustion at Mach 6 are reported herein.

1. Subsonic and supersonic combustion performance
2. Staged fuel injection
3. The effect of altitude
4. Heat transfer with combustion
5. Combustor design information

## TEST FACILITY

(U) The engine was tested at the NASA Hypersonic Tunnel Facility (HTF) at the Plum Brook Station of the Lewis Research Center. This facility is capable of true aerothermodynamic simulation of the flight environment at Mach 5, 6, and 7. The HTF incorporated a blowdown enclosed free-jet test section. The facility used an induction-heated, drilled-core graphite storage bed to raise the temperature of nitrogen to a nominal 4500°F at a maximum design pressure of 1200 psia. The nitrogen was mixed with ambient-temperature oxygen to produce synthetic air*. Diluent nitrogen was added with the oxygen in the mixer at tunnel Mach numbers below 7 to control freestream total temperature and to supply the correct weight flow to the 42 inch exit-diameter free-jet nozzles. Altitude simulation was provided by a diffuser and a single stage steam ejector as shown in Figure 1. The total length of this exhaust system was 183 ft.

(U) The test chamber was 25 ft in diameter. The facility nozzle and the diffuser duct penetrated the chamber wall through inflatable seals. A schematic of the engine and the test section is shown in Figure 2. The engine had a maximum cross-sectional area of approximately 50 percent of the facility nozzle. To improve the starting and operational characteristics, the shroud and the annular injector were installed. The shroud was used to channel the tunnel flow around the model in order to lower the test chamber pressure. The annular ejector was used to inject cold nitrogen at the nozzle exit to increase the stream momentum in the tunnel nozzle boundary layer thereby preventing flow separation. The ring attached at the shroud entrance was used to restrict the reverse flow caused by the incident shock from the engine cowl lip. In the earlier runs the tunnel diffuser was choked. This situation was circumvented by reducing the diffuser cone angle. The back pressure in some test conditions was still high enough to form a shock between the engine and shroud, making the calculation of engine external drag extremely difficult. In severe cases, the shock would cause tunnel unstart.

(U) The data recording system consisted of an analog to digital converter capable of recording 400 channels of data on magnetic tape. The sample

*Small carbon particles were observed during all tests. After one of the tests, carbon particles as large as a thumb size were found downstream of the test section. No attempt was made to assess this effect on ignition.

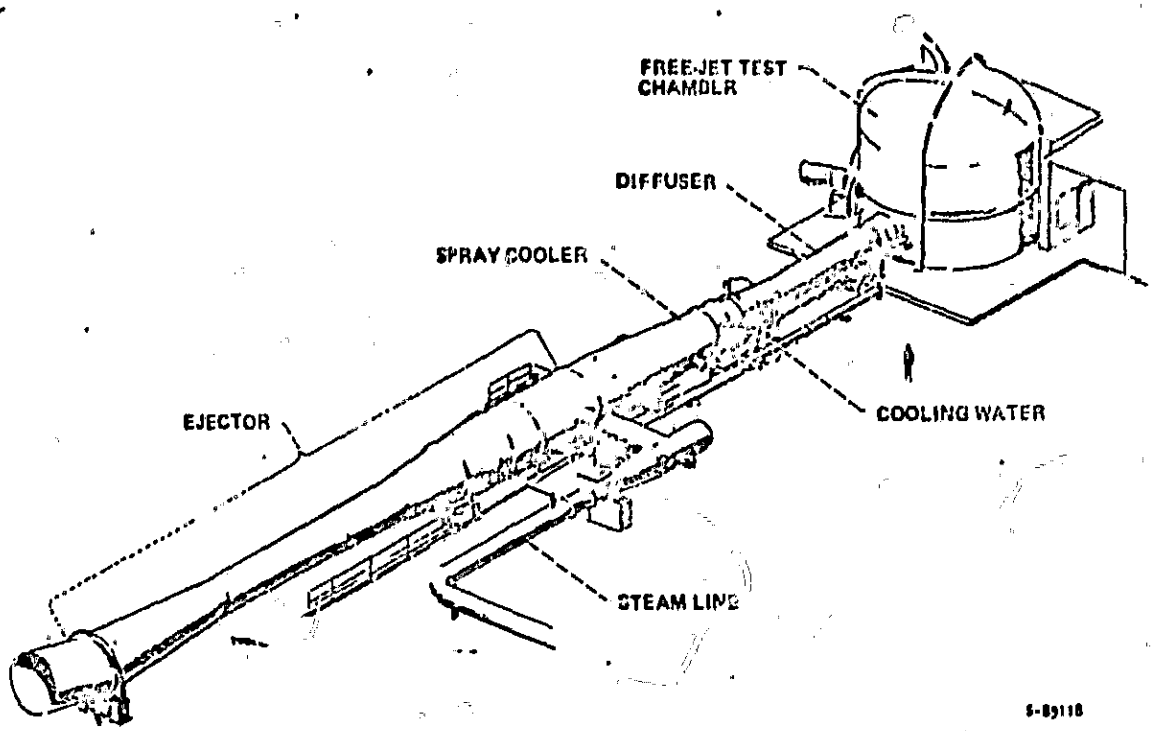


Figure 1. NASA Hypersonic Tunnel Facility
(Title, U; figure, U)

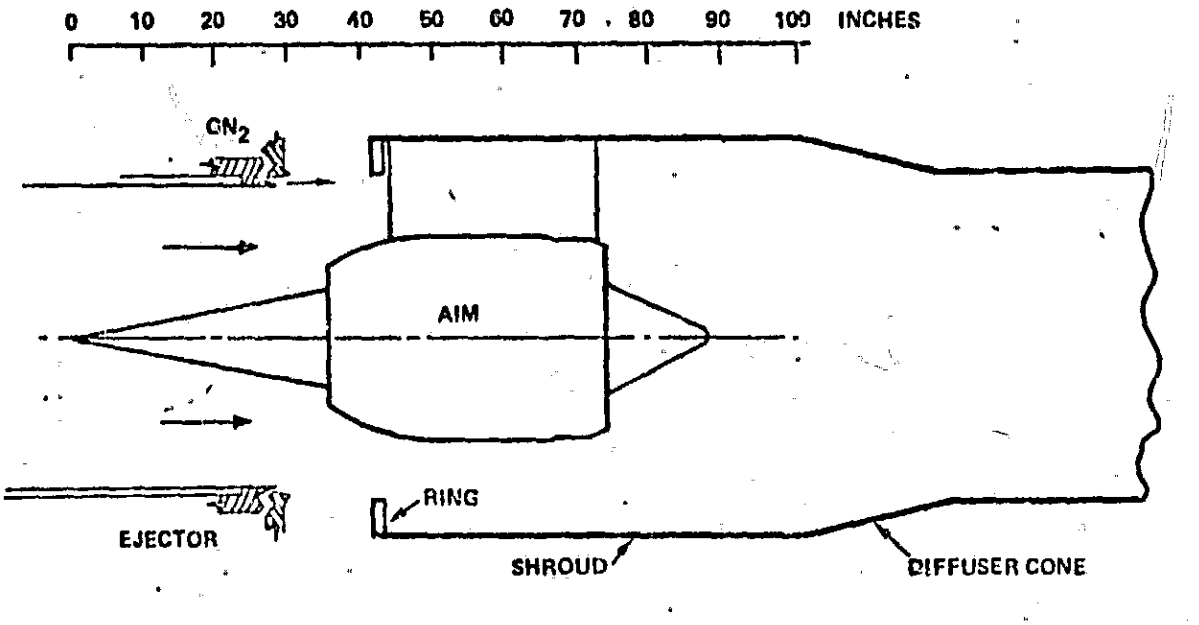


Figure 2. AIM Test Section Schematic
(Title, U; figure, U)

rate used for each channel was 5 times per second. Secondary data recording capability was provided by multi-channel oscillographs and strip-chart recorders. In addition, schlieren pictures between facility nozzle exit and shroud were displayed providing real time visual observation of tunnel operation. Motion pictures were also recorded during the run to assist in post-run analysis.

## DESCRIPTION OF AIM

(C) The Aim is axisymmetric, water-cooled and uses hydrogen fuel. Figure 3 shows the view of the engine when it was installed in the test cell. The engine consists basically of a two-shell welded structure. The shell adjacent to the hot gas was fabricated from nickel and the cold side was fabricated from steel. The tips of the spike and the cowl leading edge were made from zirconium copper. The engine weighs approximately 2200 pounds. The AIM has an inlet diameter of 18 inches, and the exit nozzle area is twice the capture area. The overall length with the translating spike in the full-forward position is 91 inches. A mixed compression inlet with variable contraction ratio was used to optimize the engine performance at different flight Mach numbers. The nozzle has a bell-shaped shroud with conical center plug. In order to minimize the correction on the internal thrust measurement, the external cowl and leg fairings are supported separately from the thrust measuring system. The hydrogen fuel was heated by passing the gas through a pebble bed heater to simulate a regeneratively cooled system.

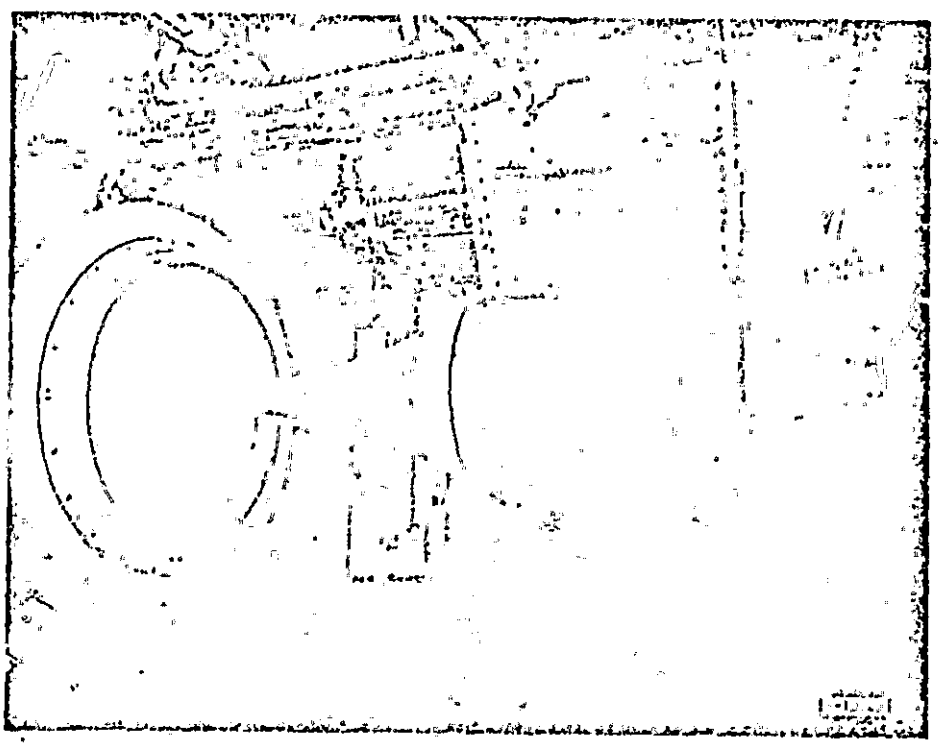

Figure 3. AIM Installed in Wind Tunnel
(Title, U; figure, U)

(U) Instrumentation included 266 pressure and 138 temperature measurements. Pressure taps were spaced every one to two inches along external and internal surfaces. Thermocouples were imbedded approximately 0.07 inches beneath the surface.

(U) There were five gas sampling probes mounted on a special rake separated from the engine assembly to measure combustor exit gas compositions. The engine internal thrust was obtained both from load cell measurements and from evaluation of surface pressure integrals.

(C) Combustor Design. The combustor schematic and area ratio distribution are shown in Figure 4 for the Mach 6 operating condition. The over all useful combustion length is 25.5 inches with an area ratio of 3.6, and consists of three combustor stages. The first combustor stage is loosely defined as the region downstream of injectors 1a and 1b, the second downstream of injectors 2a and 2c, and the third downstream of injectors 3a and 3b. The first two stages were used for supersonic combustion at higher flight Mach numbers and also for subsonic diffusion at lower Mach numbers. The third stage was used for subsonic combustion.

(C) At Mach 8, all fuel up to an equivalence ratio of one may be injected into the first stage using fuel injectors 1a and 1b. Because of spike translation, combustion occurs in a constant area section achieving maximum performance. For supersonic operation below Mach 8, fuel was to be injected into the combustor in two stages (injector 1a, 1b and 2a, 2c) in order to prevent thermal choking and inlet unstart.

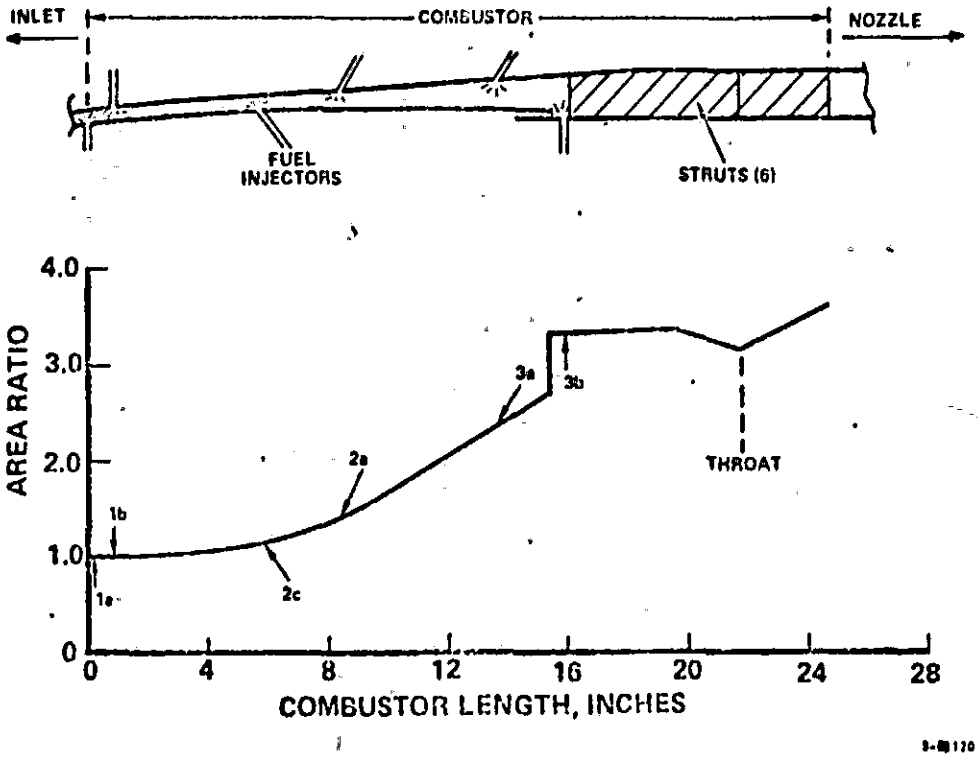


Figure 4. Combustor Area Ratio
(Title, U; figure, C)

(C) The step formed between the spike assembly and the inner shell is used as the flame stabilizer for subsonic combustion with injectors 3a and 3b. The maximum cross-section of the struts forms a geometric throat for subsonic combustion with an area reduction of five percent. The throat area was chosen to provide the best performance considering both subsonic and supersonic combustion. During subsonic combustion at Mach 4, the normal shock stabilizes near the inlet throat while at Mach 6, the shock moves downstream near the step. Because of the small restriction at the geometric nozzle throat (formed by the struts), subsonic combustion takes place at high subsonic Mach numbers. The overall subsonic combustor length is 8 inches of which 2 inches extends upstream in the second combustor section.

(C) The size and location of fuel injectors were selected to obtain desired mixing by optimizing the fuel penetration and jet spreading. The detailed injector design procedures were reported in Reference 1. As shown in Figure 4, the flows from injectors 2c, 2a, and 3a were directed upstream to increase the mixing efficiency. The injector dimensions are shown in Table I. In order to increase the mixing efficiency, the injectors in each stage were interdigitized to capture the maximum mixing area. In the final configuration, however, the injectors in the first stage (1a, 1b) were in line and opposed to each other. Consequently, mixing efficiency of the first stage was considerably reduced. The consequence of this arrangement could not be assessed.

TABLE I

AIM INJECTOR DIMENSIONS
(Title, U; table, C)

| Injector | Diameter, inches | Number | S/D | Injection Angle With Respect to AIM Centerline |
|---|---|---|---|---|
| 1a | 0.119 | 37 | 13.1 | 90° |
| 1b | 0.1205 | 37 | 13.9 | 90° |
| 2a | 0.0955 | 60 | 11.4 | 113° |
| 2c | 0.0955 | 60 | 10.6 | 119° |
| 3a | 0.091 | 114 | 7.0 | 115° |
| 3b | 0.0955 | 102 | 6.3 | 90° |

(C) Pressure Distributions. The pressure distributions on the combustor outerbody surface resulting from supersonic and subsonic combustion at Mach 6 are shown in Figure 5. The combustor inlet Mach number was 2.5 with a total temperature of 3000°R and static pressure of 15.6 psia. The bottom curve shows the pressure distribution without fuel injection. The fluctuation of this curve indicates the presence of shock waves in the combustor.

(C) The top curve depicts supersonic combustion with fuel injectors 1a, 1b and 2a, 2c. Contrary to expectations, this combination of fuel injectors produced no interaction between inlet and combustor. This lack of interaction may be because of (1) the favorable pressure gradient at the outerbody surface, (2) low flow blockage inherent in the in-line arrangement of fuel injectors 1a and 1b, and/or (3) the low static temperature (1400°R) at the inlet throat any of which could inhibit mixing and ignition. In fact, the first stage fuel-air mixture would not auto-ignite at Mach 6 even with an equivalence ratio of 0.38. The first stage fuel was ignited either by using the ignitors or by the interaction with the second stage injectors. The pressure dip at station 59 was due to expansion waves emanating from the step. The rise of pressure between the struts was because of the combined effects of shock waves and combustion. The detailed wave phenomenon will be discussed later.

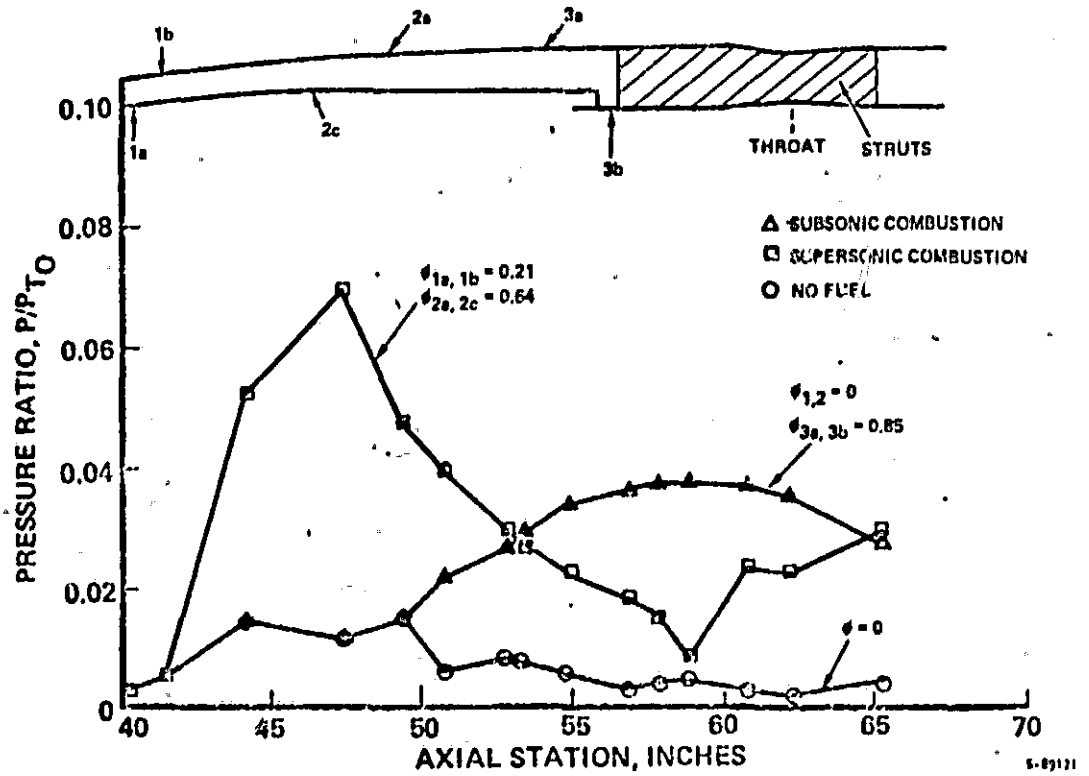


Figure 5. Static Pressure Distribution
(Title, U; figure, C)

[redacted]

(C) The subsonic combustion curve in Figure 5 has a Mach number of 2 at station 49. A normal shock at station 49 would produce a static pressure ratio of about 4.30. However, because of the large combustor throat sufficient back pressure could not be maintained to support a normal shock. Instead, the flow was diffused through one or more weak shocks to produce the observed static pressure rise of about 2 and transonic Mach numbers in the subsonic combustor stage.

(C) In order to understand the flow phenomenon inside the combustor, the test data was analyzed one dimensionally using the equations of momentum, energy, continuity and equation of state with reactants and products of combustion in chemical equilibrium. The calculation of combustor flow properties began at the freestream conditions. Using measured wall pressure integral, heat loss, and calculated friction force (Ref. 2) in the inlet, the mass-momentum-energy averaged pressure and other parameters were determined at the combustor entrance. In the combustor, the average wall static pressures were also used to define performance. The results of the analysis are shown in Figure 6. The combustor loss without heat addition upstream of station 50 was significant because of the combined effects of friction, shock and profile mixing losses. Figure 6 also shows an interesting comparison between the combustion loss and the shock loss for supersonic and subsonic combustion. During subsonic combustion, a significant portion of the loss is because of the shock loss (as shown by the discontinuous dotted line) while combustion loss is comparatively small from station 54 to 62.

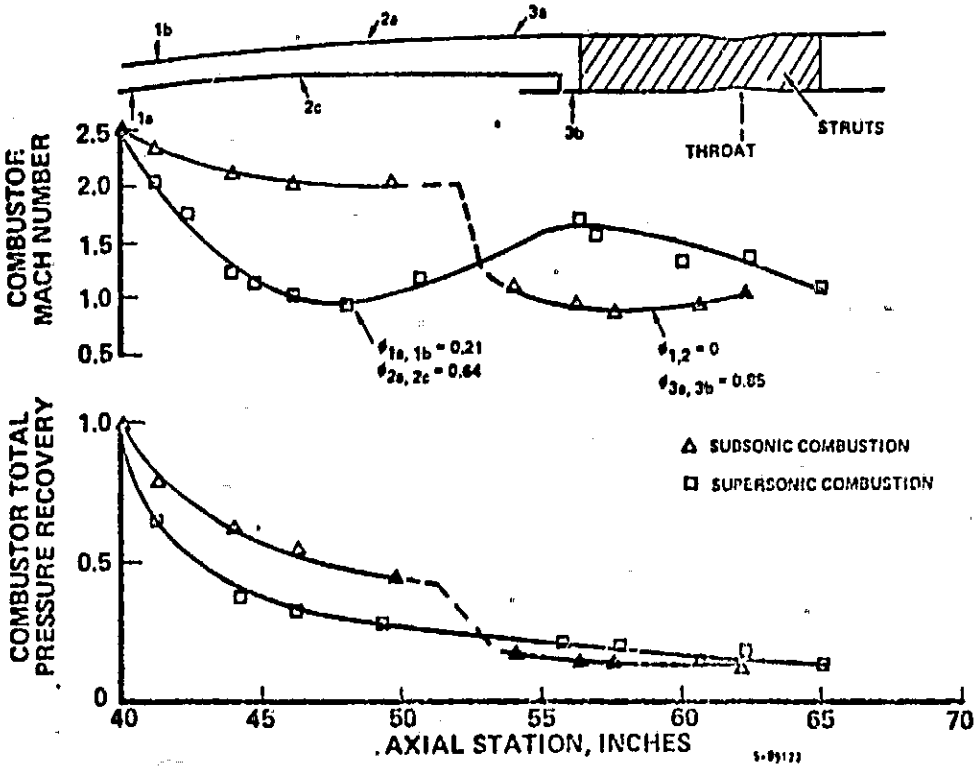


Figure 6. Combustor Flow Parameters
(Title, U; figure, C)





[redacted]

(C) Because of the small area ratio of the subsonic combustor, combustion occurred transonically unlike that of conventional subsonic combustion. There, low subsonic flow enters the combustor and burns at very low subsonic velocities. It is then accelerated to sonic velocity through a converging section. In a transonic combustor the flow may be supersonic, subsonic or a combination of both. From momentum and energy considerations, the discharge gas behaves one dimensionally like choked flow, even though the flow at the combustor exit may not be sonic uniformly.

(C) The combustion loss in the supersonic case was high, however, the overall loss between these two combustion modes was about the same. The combustion efficiencies were 81 percent and 88 percent for supersonic and subsonic combustion, respectively.

(C) Flow Field Between Struts. The static pressure drop downstream of station 56 between the struts may be explained by the expansion waves emanating from the step as shown in Figure 7. The base pressures downstream of the step correlate very well with available data (Ref. 3) considering the accuracy of flow parameters determined from this analysis. The bottom sketch shows the wave pattern when no fuel was added. The Mach number upstream of the step was 2.45. The expansion waves reflected from the c[illegible]body tended to weaken the recompression shock and bend the shock toward the center.

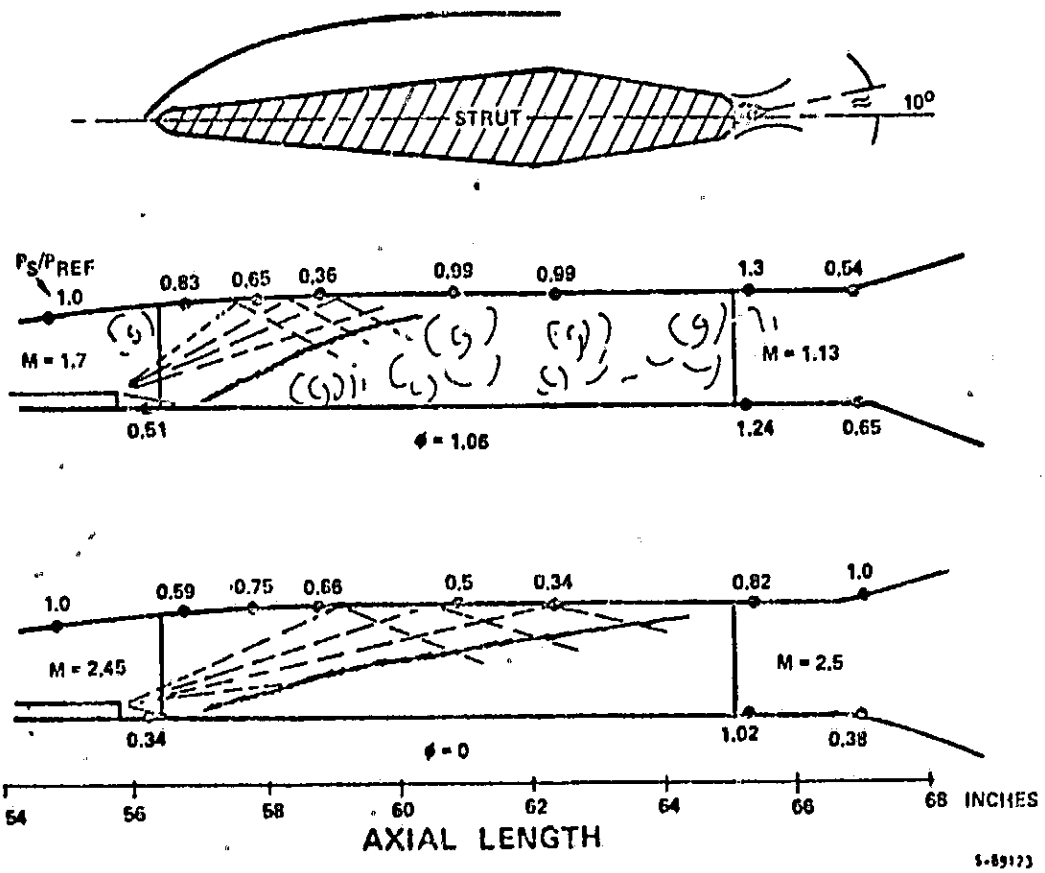


Figure 7. Effects of Struts and Steps
(Title, U; figure, C)

(C) The middle sketch shows the wave patterns between struts when fuel was injected from the first two stages. The Mach number was reduced upstream of the step to 1.7 due to heat addition. Consequently, the expansion waves were steeper. A theoretical calculation indicates that the recompression shock should strike the outerbody at a much shallower angle than that shown in this sketch. It was concluded that the static pressure rise at station 61 must be a consequence of combustion. The flow from the second stage combustor may have been quenched by the expansion waves and again ignited by the recompression shock. The combustion is very similiar to a shock induced combustion process which would cause the recompression shock to assume a steeper angle due to increased back pressures. This is possible if the flow normal component downstream of the shock is subsonic. This conclusion was further substantiated by the increased wall temperatures as discussed below.

(U) The strut leading edge shock from the observed heat patterns on the skin is shown on the top sketch. Metal surface heat patterns in the wake downstream of the strut showed a counterclockwise swirl of approximately 10 degrees. This swirl was also observed by inspecting the leading edge of the struts which showed a similar counterclockwise swirl. It is possible that this swirl can seriously impair the nozzle performance because the nozzle gross thrust is directly proportional to the cosine of the flow angularity. It is speculated that the swirl may be caused by non-uniform combustion which is usually associated with a highly intensified combustion process.

(U) Combustor Stage Interaction. Fuel from injectors 1b, 2a, and 2c (Case 1) was compared with that from injector combination 1b, 3a, and 3b (Case 2) in Figure 8 at an equivalence ratio near unity. In Case 1 only supersonic injectors were used whereas in Case 2 the subsonic injectors are used along with upstream injector 1b.

(C) A strong interaction between injectors 1b, 2a, and 2c can be seen by comparing the outer wall pressure rise prior to station 46. Although the fuel injected from 1b is approximately the same, Case 1 has a pressure rise twice that of Case 2.

(C) In this run, no ignitors were used. The first stage was ignited by the interaction with second stage injectors. The first stage would stay ignited after second stage fuel was decreased. Then the first stage combustion would cause the third stage fuel-air mixture to ignite as shown in Case 2.

(C) The boundary layer separation produced by the second stage jets behaved as a wedge forming oblique shocks. The pressure rise behind these shocks propogated upstream to ignite the first stage.

(C) A further insight as to what process occurred in these two cases can be seen in Figure 9 where calculated combustor Mach number and total pressure recovery were plotted versus axial location. Without fuel injection, total pressure decreased smoothly due to shock, profile and friction losses. In the first six inches, about 50 percent of the combustor inlet total pressure was lost.

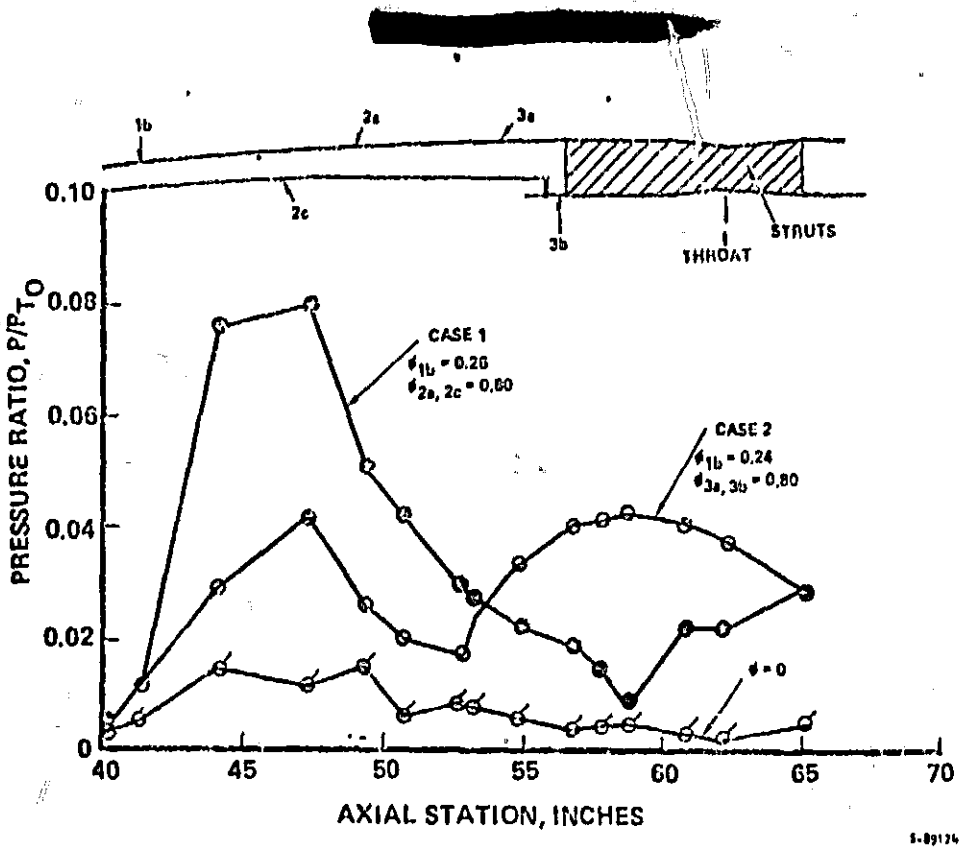


Figure 8. Static Pressure Distribution
(Title, U; figure, C)

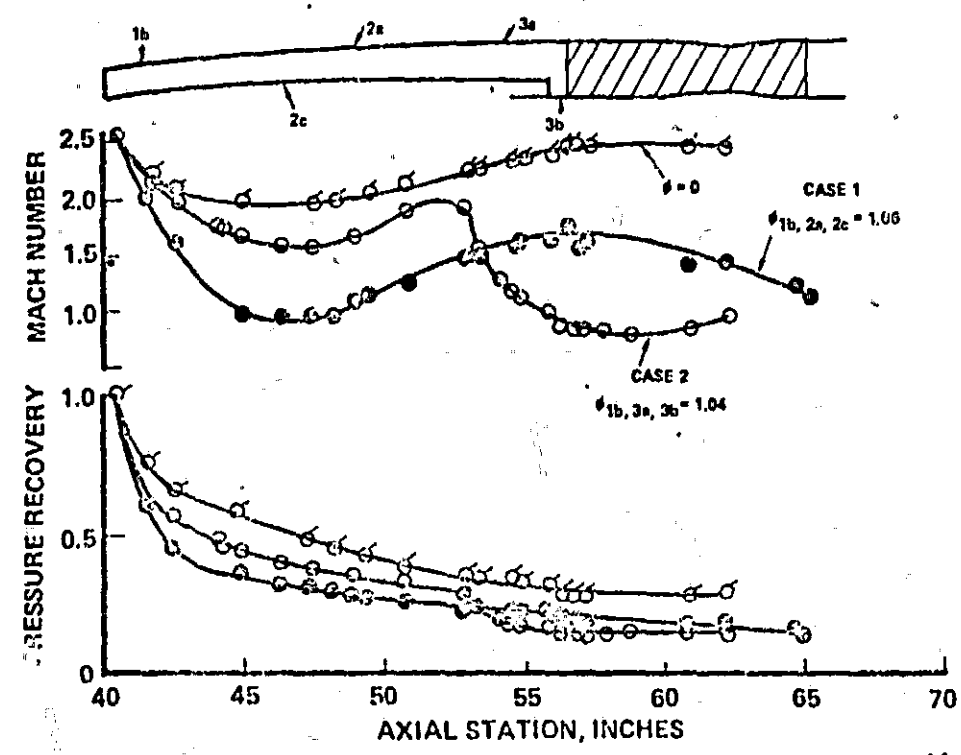


Figure 9. Combustor Flow Parameter
(Title, U; figure, C)

(C) In Case 1, however, a strong shock system set up by the interaction of 1b with 2a and 2c caused a steep total pressure loss curve in the first few inches of combustor length. This shock system was so strong that 50 percent of the total pressure was lost in just 1.6 inches of combustor length.

(C) The interaction between injectors 1b, 2a, and 2c produced transonic Mach numbers in the constant area section. The flow remained transonic past injector 2c and then gradually the Mach number increased in the diverging area due to mixing and combustion. If all of the injected fuel had burned prior to the combustor step, then a Mach number distribution similar to that at an equivalence ratio of 0 would be expected past station 56. However, further combustion in the strut region decreased the Mach number to about 1.15 at the strut trailing edge.

(C) Without strong injector interaction in Case 2, the combustion in the first stage was not as complete as in Case 1. The Mach number remained supersonic in the constant area section and then accelerated as the flow area increased. Because of the combustion of fuel from injectors 3a and 3b, the flow was reduced to subsonic Mach numbers then accelerated to Mach 1 at the throat.

(C) Case 2 has a combustion efficiency of only 81 percent compared with 96 percent in Case 1. Mixing near an equivalence ratio of one is difficult and required 24 inches of combustor length to almost completely burn the injected fuel in Case 1. Apparently the 8 inch length provided for subsonic combustion was too short for fuel to mix and completely burn.

(C) A calculation of flow residence time in the combustor indicates that there is only 500 μsec available for the fuel to mix, ignite and react. During subsonic combustion in Case 2, the combustor residence time is reduced by one-half, even though average velocities are lower, since the total combustor length is 8 inches compared with 24 inches in Case 1.

(C) Combustion Efficiency. Combustor efficiency ($\eta_c$) versus axial station is shown in Figure 10 for the case of supersonic combustion with fuel injection from 1b, 2a and 2c at a equivalence ratio of 1.06 (Case 1 in previous discussion). Combustor efficiency is defined as the mass fraction of injected fuel reacted in equilibrium required to satisfy the one-dimensional conservation equations.

$$\eta_c = \frac{\dot{W}_{H_2} \text{ reacted}}{\dot{W}_{H_2} \text{ injected}}$$

The fuel from injector 1b mixed and burned rapidly reaching 74 percent efficiency in 4 inches. The overall efficiency decreased when additional fuel was injected from 2c and 2a. The efficiency plot in the region between injector 1b and 2a is shown dashed since the flow was not truly one dimensional as evidenced by wide variations in lower and upper wall pressures. Once past this region, the flow was more uniform and thus the one-dimensional calculations were more representative.

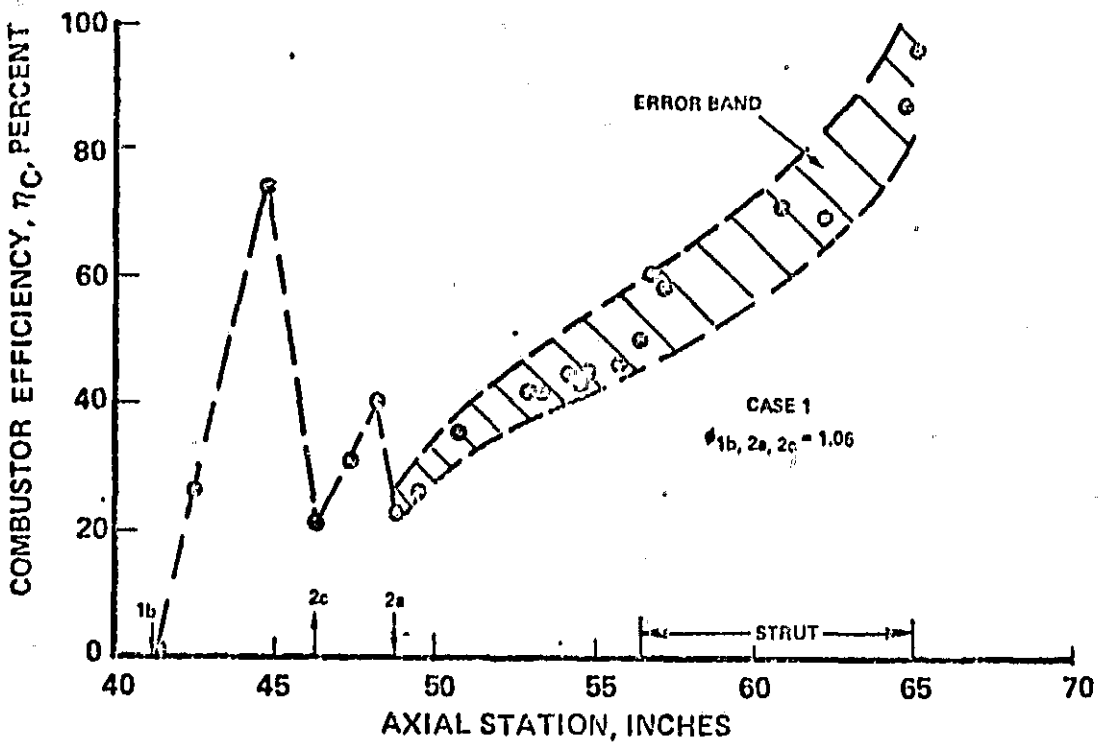


Figure 10. Supersonic Combustor Efficiency (Title, U; figure, C)

(U) An error band is shown around the mean of the efficiency calculations. This band was based on an error analysis which included the inaccuracies of measured flow, wall static pressures, and heat loss along with errors in calculating the combustor pressure integral (Ref. 4).

(U) It should be noted that there is a large scatter in the calculations in the strut region because of the method of calculating the strut force. For lack of measured pressures on the strut itself, the strut force was calculated from measured wall static pressures between struts and was linearly distributed along its length.

(C) The combustion efficiency distribution for Case 2 with fuel injection from 1b, 3a and 3b is given in Figure 11. Note that the slope of combustion efficiency of fuel from 1b is not as steep as in Case 1 (Figure 10). Also there was a delay of about an inch before any combustion occurred.

(U) Combustor Performance Parameters. Combustion efficiency alone is not sufficient to completely define the performance of a supersonic combustor. The availability of energy to produce thrust must also be defined. The combustor total pressure loss in conventional subsonic combustion ramjets is not high, with most of the loss occurring in the inlet. In supersonic combustion a considerable total pressure loss occurs during combustion.

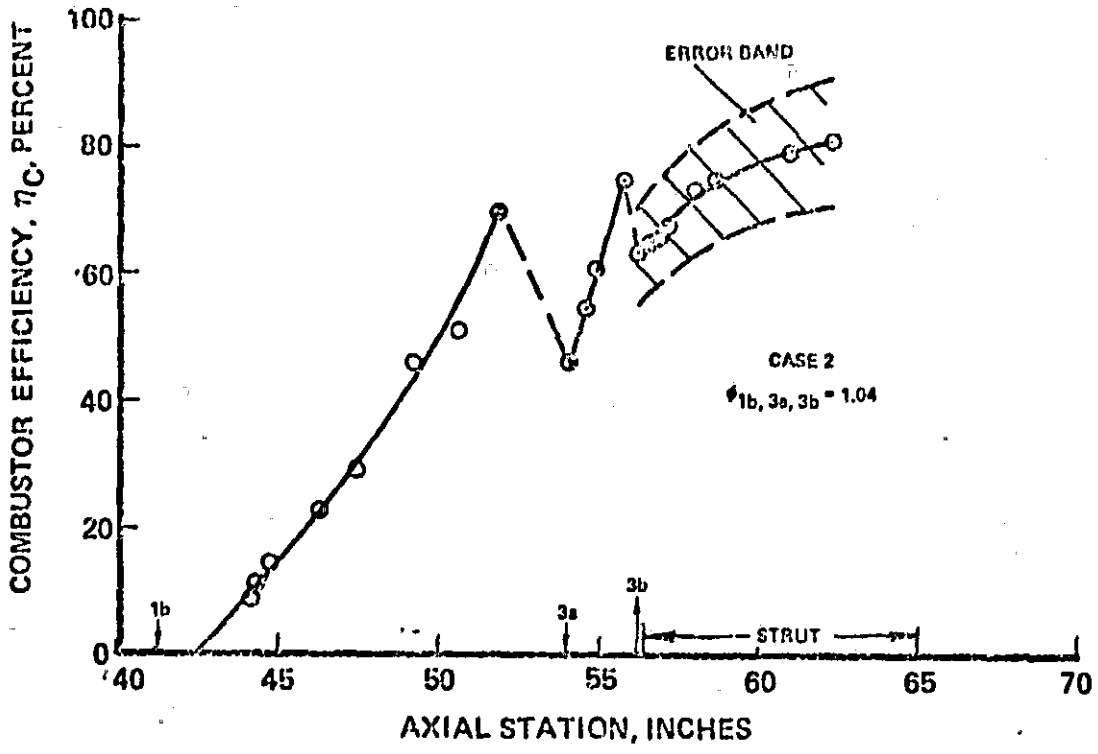


Figure 11. Super/Subsonic Combustor Efficiency
(Title, U; figure, C)

(C) The sensitvity of combustor total pressure recovery with effective equivalence ratio is shown in Figure 12. Examination of the data shows a small variation in total pressure recovery with wide variations in effective equivalent ratio and injector configuration. However, small changes in combustion exit total pressure can produce large changes in engine thrust. Combustor exit total pressure is also difficult to measure directly. Therefore, the use of measured or calculated total pressure recovery to define a combustion process was assumed impractical.

(U) The Crocco pressure-area relationship assumes that combustor pressure varies exponentially with area (Ref. 5). The equation is

$$P\,A^{\frac{\epsilon}{\epsilon - 1}} = \text{constant}$$

$$\text{with} \quad \int PdA = (1 - \epsilon)\,(P_{exit}A_{exit} - P_{inlet}A_{inlet})$$

where $\epsilon = 0$ = constant pressure process

$\epsilon = 1$ = constant area process

$\epsilon = \gamma M^2$ = constant Mach number process

Once $\epsilon$ is defined, both combustor exit static pressure and the pressure integral $\int PdA$ are also defined. The problem with this correlation is that

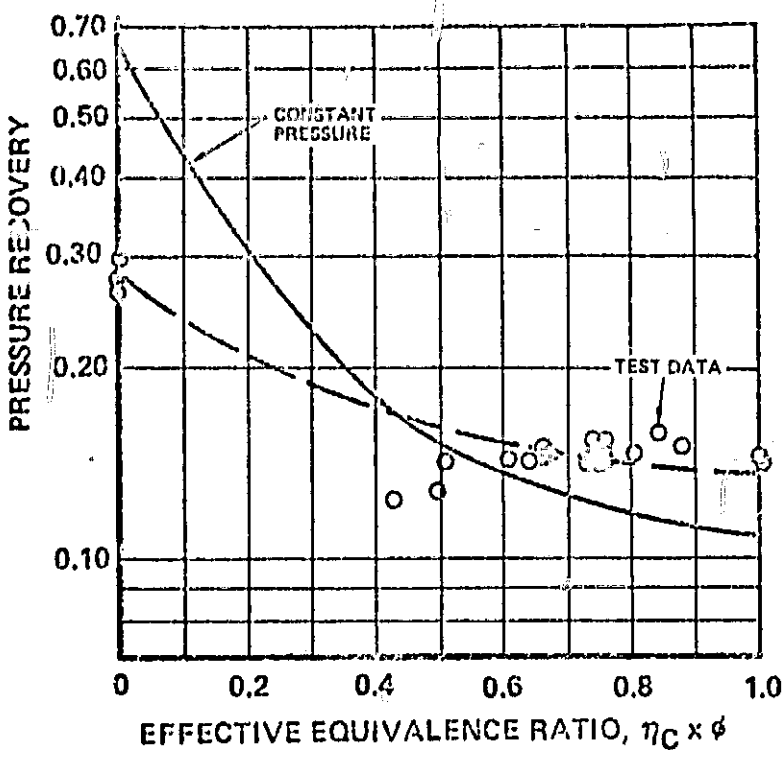


Figure 12. Total Pressure Recovery
(Title, U; figure, C)

the pressure varies monotonically with the area. It implies that the area ratio alone will determine the pressure distribution. In an actual combustor, the pressure distribution is strongly affected by the injection, mixing, and chemistry process as well as the combustion geometry.

(C) The actual combustion process in a diverging combustor could not be expressed by this simple equation. In fact, two different values of $\epsilon$ are required to represent the actual combustion process--one to match the value of $\int PdA$ and the other to match the static pressure at the combustor exit. For a typical example, to match the value of $\int PdA$ in AIM data required an $\epsilon$ of 0.07, whereas combustor exit static pressure was matched at an $\epsilon$ of 0.2. Therefore, the assessment of combustor process using a single value of $\epsilon$ is not practical.

(U) Another parameter used to determine the combustion process is the pressure-area integral factor, K, defined as

$$K = \frac{\int PdA}{\frac{1}{2}\left(P_{exit} + P_{inlet}\right) \Delta A}$$

Unlike the Crocco relationship, a single value of K would be able to match the thrust and pressure from test data and completely define the combustor exit condition.

(U) The K factor was calculated from several of the AIM tests having different injector configurations and presented in Figure 13 as a function of effective equivalence ratio. Very good correlation was obtained for these Mach 6 tests because overall combustor losses did not vary significantly with injector configuration.

(U) Finally, a single parameter which may be used to indicate the performance of a supersonic combustor is the Combustor Effectiveness. It is defined as:

$$\eta_{ce} = \frac{(1 + f/a)\, I_{vac_{am}} - I_{vac_2}}{(1 + f/a)\, I'_{vac_{am}} - I_{vac_2}}$$

Where $I_{vac_2}$ = combustor entrance vacuum specific impulse

$I_{vac_{am}}$ = actual combustor exit vacuum specific impulse expanded isentropically to ambient pressure

$I'_{vac_{am}}$ = combustor exit vacuum specific impulse for constant pressure, zero velocity-combustion expanded isentropically to ambient pressure

Of course, 100 percent ideal combustor effectiveness will never be reached because the heat addition loss (Raleigh loss) is assumed to be zero for the ideal thrust calculation.

(C) The Combustor Effectiveness was calculated and plotted as a function of equivalence ratio and presented in Figure 14. It appears that for all of the various injector configurations used, $\eta_{ce}$ varies between 0.7 and 0.9. It has the advantage of using a single parameter to indicate the thrust producing potential of the combustor. The highest combustor effectiveness in Figure 14 corresponds to the maximum measured thrust.

(C) Altitude Effect. The effect of altitude on measured wall static pressure is shown in Figure 15. At a freestream total pressure of 925 and 750 psia (76,000 and 81,000 ft altitude simulation) the pressure distribution and calculated combustor efficiencies (90%) were almost identical. At 470 psia (91,000 ft altitude simulation) the pressure distribution and the calculated combustor efficiency (65%) was significantly lower than at 750 or 925 psia because of the chemical kinetic effect of hydrogen-air combustion at low pressures. The residence time of mixture in the combustor was approximately equal to the ignition delay time. A detailed discussion of this phenomenon is discussed in Reference 6.

(C) Temperature Distributions and Heat Losses. The thermocouple temperatures in the combustor also provide some indication of combustion as shown in Figure 16. For clarity, only the outerbody temperature is shown. The estimated skin surface temperature based on water temperature and skin thickness is also presented. The maximum calculated

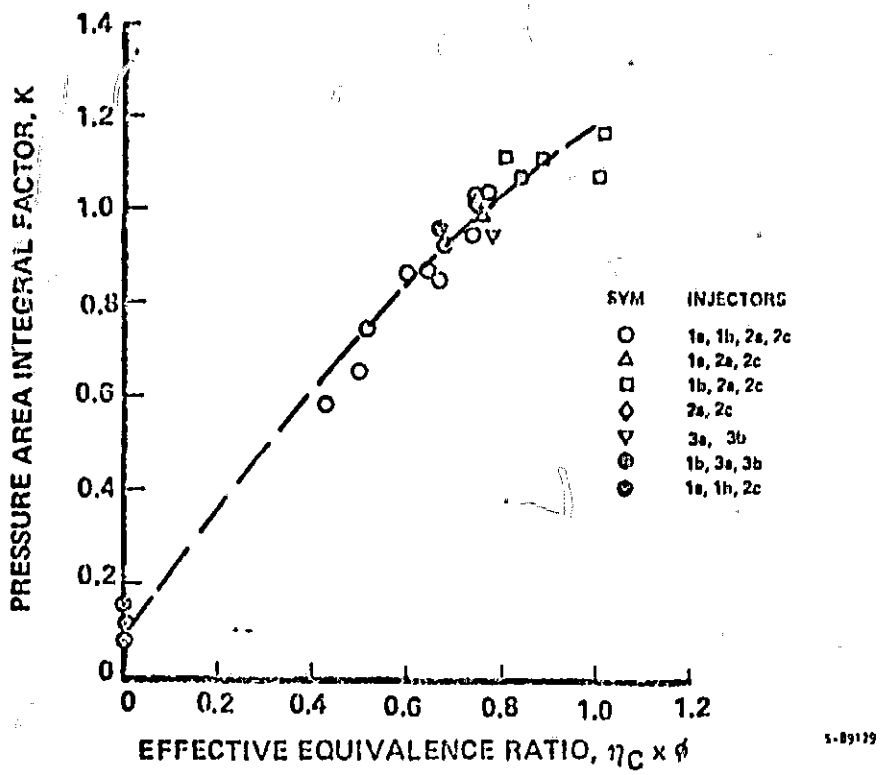


Figure 13. Combustor Pressure Area Integral Factor
(Title, U; figure, C)

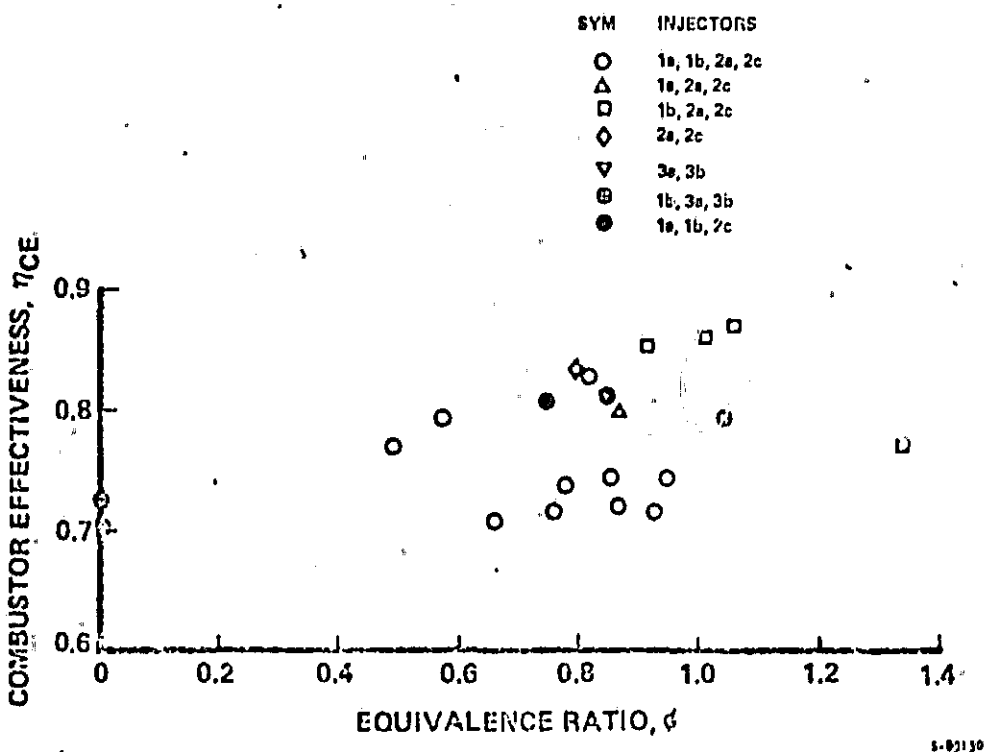


Figure 14. Combustor Effectiveness
(Title, U; figure, C)

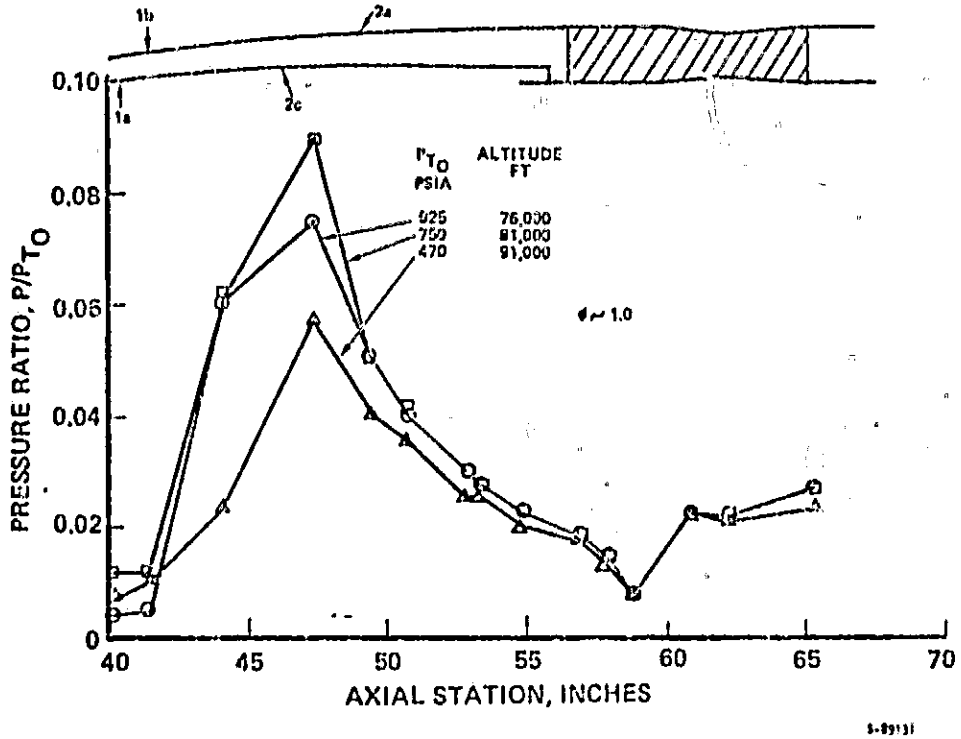


Figure 15. Altitude Effects
(Title, U; figure, C)

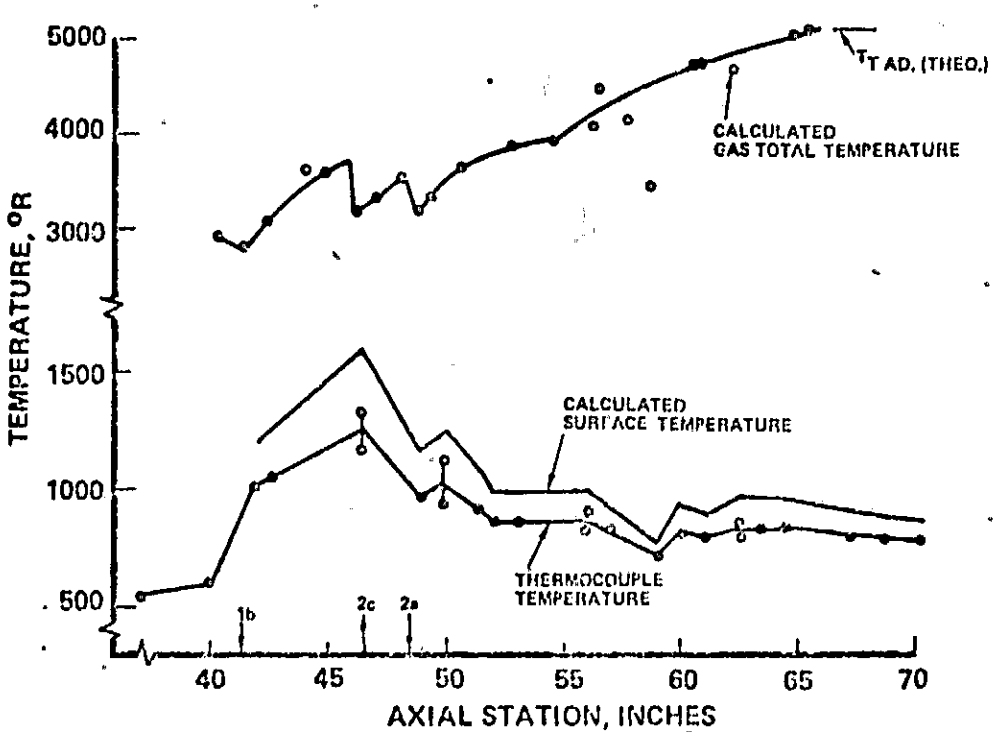


Figure 16. Temperature Distribution
(Title, U; figure, C)

surface temperature of 1600°R occurred at the second stage injector station which corresponds to the peak pressure rise. The increase of surface temperature both on the outer body and on the inner body downstream of station 60 further substantiates the combustion phenomenon between the struts. The temperature rise between struts was not observed with no fuel injection.

(U) The average of the calculated total gas temperature in the combustor is shown on the top curve in Figure 16. This temperature was calculated from the one-dimensional flow model discussed above. The theoretical adiabatic combustion temperature is also shown. The close agreement between the calculated temperature and the theoretical adiabatic temperature indicates that the combustor heat loss and the energy gain by heating up the fuel is about the same, which is necessary in simulating a regeneratively cooled system.

(C) Figure 17 shows the theoretically calculated engine cooling load for Case 1 as compared with the measured heat loss. The measured heat loss distribution was determined from overall cooling water temperature rise and the skin thermocouple temperature distribution. This method was considered to be more reliable than measuring the water temperatue rise at many points in the engine as originally planned. The maximum local averaged heat flux was 355 Btu/sec-ft$^2$ at the second stage fuel injection station. The average heat flux for the combustor was 200 Btu/sec-ft$^2$. The stagnation heat flux for the strut leading edge was 1711 Btu/sec-ft$^2$ as compared with a theoretical design value of 1890 Btu/sec ft$^2$ calculated

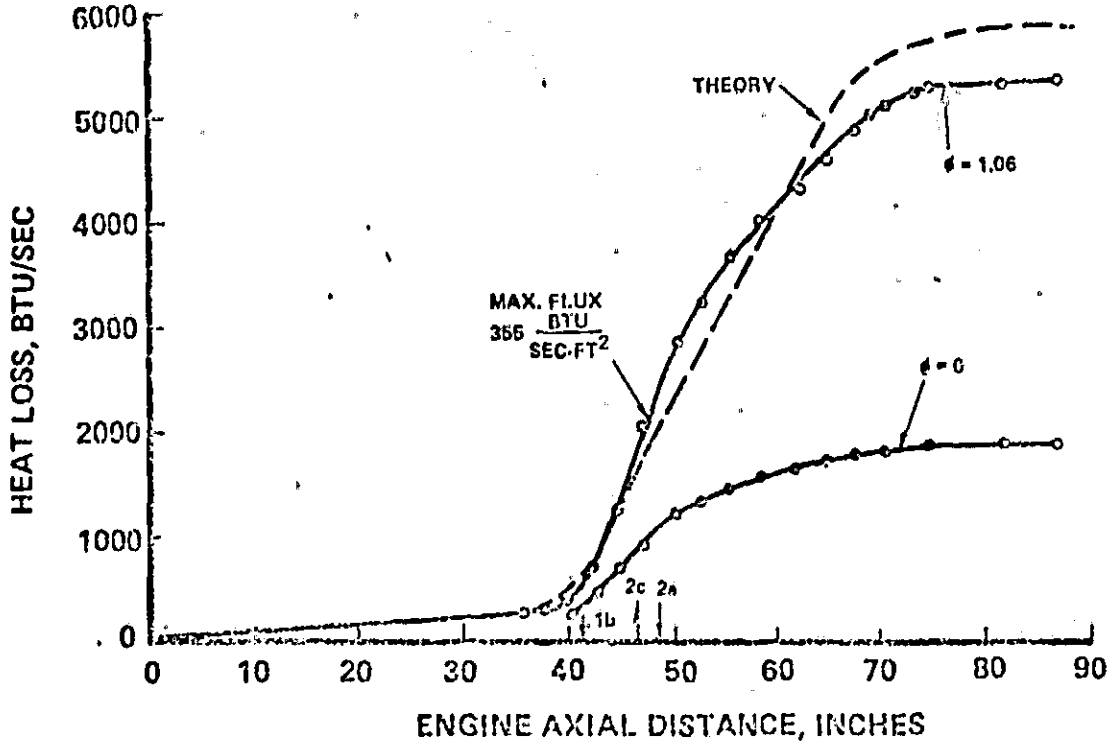


Figure 17. Heat Loss Distribution
(Title, U; figure, C)

at a slightly different operating condition. The calculated overall heat load is in good agreement with average experimental data. The close agreement in the total heat load has increased confidence in future engine designs.

(U) Combustor Design Information. Table II presents realistic design information based on Mach 6 AIM tests. The injector discharge coefficient is dependent on pressure ratio and thus there is a wide variation. The peak combustion efficiency varies with injector configuration, and the range shown is based on an error analysis.

TABLE II

COMBUSTOR DESIGN INFORMATION
(Title, U; table, C)

| | Test Result |
|---|---|
| Fuel injector discharge coefficient | 0.6 to 0.85 |
| Auto ignition (first stage) | No |
| Stage interaction | Strong |
| First stage unstart (equivalence ratio) | 0.35 |
| Average combustor heat flux | 200 Btu/sec-ft$^2$ |
| Average friction coefficient | 0.0030 |
| Peak combustion efficiency | 0.8 to 1.0 |
| Pressure integral factor (K) at $\phi = 1$ | 0.9 to 1.2 |

## CONCLUSIONS

(C) The preceding discussion of AIM test data supports the following conclusions:

1. Stable supersonic and subsonic operation was achieved at Mach 6 in a ground test facility simulating a true flight environment.

2. Realistic supersonic combustion performance was obtained with combustor efficiencies up to 95 percent and combustor effectiveness between 70 percent and 87 percent.

3. Subsonic and supersonic combustion performances were about the same due to the design compromise on the nozzle throat area and combustor length.

[redacted]

4. The interaction effects in staged fuel injection proved very important in achieving auto-ignition, high combustor efficiencies and overall performance.

5. Hydrogen-air combustion was sensitive to altitude. Significant reduction in combustion efficiencies was observed at 91,000 feet altitude.

6. Close agreement between predicted and measured total cooling load has increased confidence in future engine design.

7. Combustor design parameters obtained from the Mach 6 tests confirmed most of the values used in the original design. However, the strong stage interaction effects discovered during these tests will be used to great advantage in any future designs.



[redacted]

## REFERENCES


Reference 1 — Engineering Staff, Hypersonic Research Engine Project - Phase II, Aerothermodynamic Integration Model Development Seventh Interim Technical Data Report, 10 September through 9 December 1969, NASA Contract No. NAS1-6666, AiResearch Document No. AP-69-5899.

Reference 2 — Spalding, D. B., and S. W. Chi, "Drag of a Compressible Turbulent Boundary Layer on a Smooth Flat Plate With and Without Heat Transfer", Journal Fluid Mechanics, Vol 18, pt. 1, Jan 1964, pp. 117-143.

Reference 3 — Korst, H. H., "A Theory for Base Pressure in Transonic and Supersonic Flow", Journal of Applied Mechanics, Vol. 23, 1956.

Reference 4 — Engineering Staff, Hypersonic Research Engine Project - Phase II, Aerothermodynamic Integration Model Measurement Plan, NASA Contract No. NAS1-6666, AiResearch Document No. AP-70-6216, 9 June 1970.

Reference 5 — Crocco, L., One-Dimensional Treatment of Steady Gas Dynamics, Fundamentals of Gas Dynamics, Vol. III of High Speed Aerodynamics and Jet Propulsion, Princeton University Press, 1958.

Reference 6 — Engineering Staff, Hypersonic Research Engine Project - Phase II Chemical Kinetics Study for a Supersonic Combustor Model, NASA Contract No. NAS1-6666, AiResearch Document No. AP-70-6319, 20 May 1970.